Available online at www.sciencedirect.com
ScienceDirect
Biomaterials 28 (2007) 3055–3062
Biomaterials
www.elsevier.com/locate/biomaterials

Si–C linked oligo(ethylene glycol) layers in silicon-based photonic crystals: Optimization for implantable optical materials

Kristopher A. Kilian[a], Till Böcking[a,b], Katharina Gaus[c], Michael Gal[b], J. Justin Gooding[a,*]

[a]School of Chemistry, University of New South Wales, Sydney, NSW 2052, Australia
[b]School of Physics, University of New South Wales, Sydney, NSW 2052, Australia
[c]Centre for Vascular Research, School of Medical Sciences, University of New South Wales, Sydney, NSW 2052, Australia

Received 11 January 2007; accepted 9 March 2007
Available online 18 March 2007

Abstract

Porous silicon has shown potential for various applications in biology and medicine, which require that the material (1) remain stable for the length of the intended application and (2) resist non-specific adsorption of proteins. Here we explore the efficacy of short oligo(ethylene glycol) moieties incorporated into organic layers via two separate strategies in achieving these aims. In the first strategy the porous silicon structure was modified in a single step via hydrosilylation of α-oligo(ethylene glycol)-ω-alkenes containing three or six ethylene glycol units. The second strategy employs two steps: (1) hydrosilylation of succinimidyl-10-undecenoate and (2) coupling of an amino hexa(ethylene glycol) species. The porous silicon photonic crystals modified by the two-step strategy displayed greater stability relative to the single step procedure when exposed to conditions of physiological temperature and pH. Both strategies produced layers that resist non-specific adsorption of proteins as determined with fluorescently labelled bovine serum albumin. The antifouling behaviour and greater stability to physiological conditions provided by this chemistry enhances the suitability of porous silicon for biomaterials applications.

Keywords: Porous silicon; Photonic crystals; Self-assembled monolayers; Protein resistance; Oligo(ethylene glycol)

1. Introduction

Porous silicon, a promising biomaterial [1–4] and biosensor component [5–11], is formed by anodic etching of single crystal silicon. As a photonic crystal sensor it has been used to detect the presence of gases/liquids [12–16] and biomolecules in aqueous media [5–11]. These types of sensors are based on the changes in the refractive index of the material resulting from the infiltration of molecular species into the pores of the structure.

While freshly etched PSi exhibits the requisite optical properties to transduce a biorecognition event, degradation of the material by surface oxidation has impeded wide-scale employment. The freshly etched surface contains silicon hydride species that are prone to attack by oxygen and water, a particular problem for applications requiring aqueous stability. To combat this problem, protection strategies have been developed using surface chemistry approaches such as self-assembled alkyl silanes [5,7,8,10] and alkene hydrosilylation [17–23]. Hydrosilylation of alkenes has been shown many times to result in monolayers via Si–C bonds, which are not prone to hydrolysis or the formation of multilayers (a problem with silane chemistry) [17]. The ability of organic layers to passivate the surface is only one of the criteria that the surface chemistry must satisfy to make PSi photonic crystals suitable for sensing. The ability of the monolayer to resist non-specific effects is an equally important property. Since the pioneering work of Whitesides et al. [24], oligo(ethylene glycol) (OEG) moieties in self assembled monolayers have proven a robust and versatile approach to combat non-specific adsorption. The interest in silicon as a sensor material has led to significant research effort into employing OEG molecules in conjunction with hydrosilylation chemistry [22,25–32]. Cai [26] and Hamers [30] have independently

*Corresponding author. Tel.: +61 2 93855384; fax: +61 2 93856141.
E-mail address: justin.gooding@unsw.edu.au (J.J. Gooding).

0142-9612/$ - see front matter © 2007 Elsevier Ltd. All rights reserved.
doi:10.1016/j.biomaterials.2007.03.014

reported evidence for improved resistance against non-specific adsorption of proteins on silicon with increasing number of ethylene glycol (EG) units. EG_3 containing monolayers were found to be protein resistant on gold but failed to adequately protect silver and silicon surfaces [29,33]. Work by Herrwerth et al. [34] on metal surfaces confirmed the importance of chain conformation in protein resistance and attributed protein resistance to internal and external hydrophilicity (via water binding within OEG chains and terminal hydroxyl groups). The effect of substrate on chain conformation underscores the importance of understanding the underlying surface and structural morphology of a given system. While detailed studies have been conducted on flat silicon surfaces, little attention has been devoted to protein resistance with OEG layers in porous silicon, a material with very different surface structure and morphology. The purpose of the work presented here is to evaluate the stabilization and antifouling properties of different OEG layers on PSi photonic crystals. The type of photonic crystal employed in this study is the so-called rugate filter, which is characterized by a narrow reflectivity peak. Such devices are achieved by generating a sinusoidal refractive index profile along the optical axis of the structure, as was described previously [35]. In our devices, the optical resonance was tuned to the near infrared spectral region (700–1000 nm) so as to be practical in applications involving transmission through tissue [36] and hence be amenable to implantable devices for non-invasive interrogation.

To develop a suitable strategy for protecting the underlying silicon surface from oxidation whilst resisting non-specific protein adsorption, we used a single step method reported previously [22,25–32] as a starting point. Hydrosilylation of undecenyl tri(ethylene glycol) and undecenyl hexa(ethylene glycol) monomethyl ethers ($C11EG_nMe$, $n = 3$, 6) are compared to dodecene (C12) as a model hydrophobic interface for protein adsorption within the porous filter (Fig. 1, Strategy 1, Surfaces (1)–(3)). This strategy incorporates the alkyl tail for monolayer packing with the protein resistant OEG moiety in a single reaction step. We also explore an alternative two-step procedure that employs (1) hydrosilylation of succinimdyl-10-undecenoate (NHS undecenoate) to form a dense alkyl monolayer and (2) subsequent coupling of an amino

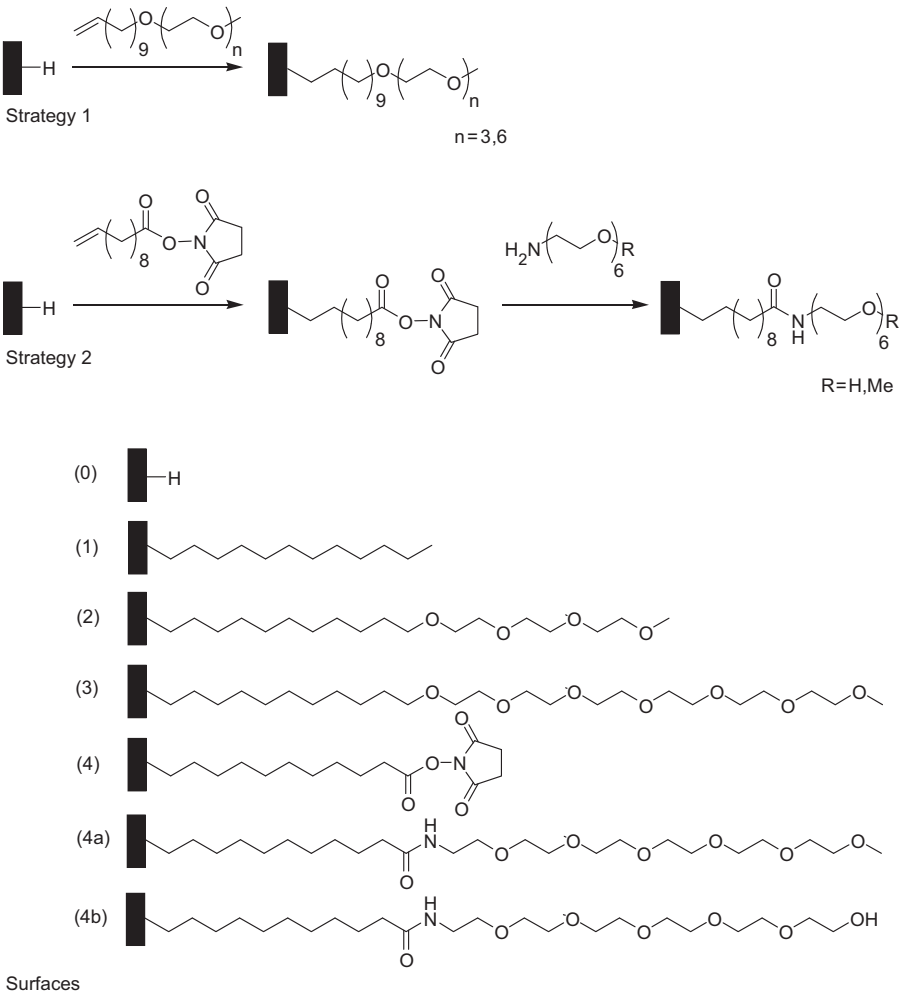

Fig. 1. Top: strategies for molecule immobilization to prepare Si–C linked bioresistant layers on porous silicon optical filters. Bottom: prepared surfaces used in stability and protein resistance studies.

modified hexa(ethylene glycol) (H_2NEG_6R, R = Me, H) to the active NHS terminus (Fig. 1, Strategy 2, Surface (4a)/(4b)) to impart antifouling behaviour [23]. A comparison of the interfaces produced by these different strategies has not previously been reported and may provide insight into factors that effect aqueous stability and non-specific protein adsorption. Towards this understanding, the characteristics of both chemistries were explored in detail and the suitability to passivate the underlying silicon surface, thus slowing physiological degradation whilst reducing the non-specific adsorption of proteins was investigated and compared.

2. Materials and methods

2.1. Chemicals and materials

All chemicals were reagent grade or higher and purchased from Sigma-Aldrich (Sydney, Australia). Mesitylene (1,3,5-trimethylbenzene) and 1,3,5-triethylbenzene were redistilled from sodium and subsequently stored over molecular sieves until use. Si(1 0 0) wafers, B-doped, resistivity 0.005 Ω cm were purchased from the Institute of Electronics Materials Technology (ITME, Warsaw, Poland).

2.2. Synthetic methods

2.2.1. Undecenyl OEG monomethyl ethers ($C11EG_nMe$ ($n = 3, 6$))

$C11EG_3Me$ was prepared as described previously [32]. $C11EG_6Me$ was prepared in four steps from hexa(ethylene glycol). First the mono-protected hexa(ethylene glycol) derivative, 1-*tert*-butyldimethylsilylhexa(ethylene glycol) (TBDMS-EG_6) was prepared by adding triethylamine (15 mmol), dimethylaminopyridine (DMAP) (0.15 mmol) and *tert*-butyldimethylsilylchloride (TBDMSCl) (15 mmol) to a solution of hexa(ethylene glycol) in dry dichloromethane (15 mmol/30 mL) and stirring the resulting mixture at room temperature overnight. The solvent was removed under reduced pressure and the residue purified using column chromatography on silica (ethyl acetate:acetone 2:1) to give TBDMS-EG_6 as a colourless oil. Sodium hydride (30 mmol) was added to a stirred solution of TBDMS-EG_6 in dry THF (15 mmol/30 mL) at 2–8 °C and the solution was stirred until gas evolution halted (circa. 15 min). Methyl iodide (15 mmol) was added dropwise over 5 min and the reaction was allowed to warm to room temperature and stirred overnight. The crude mixture was partitioned between ethyl acetate (50 mL) and brine (50 mL), the organic phase was washed with water (2 × 50 mL), dried over sodium sulphate and the solvent was removed under reduced pressure. The silyl protecting group was removed through stirring the protected methyl ether with dilute hydrochloric acid (1% v/v, 10 mL/3 mmol) for 1 h. The volatiles were removed under reduced pressure to yield the crude hexa(ethylene glycol) monomethyl ether. This crude product was then treated with sodium hydride (30 mmol) in THF (15 mmol/30 mL) on ice for 15 min. 11-Bromoundec-1-ene (18 mmol) was added in small portions and the reaction was allowed to warm to room temperature and stirred overnight. The solvent was removed under reduced pressure and the crude product was purified using column chromatography on silica (ethyl acetate) to yield undecenyl hexa(ethylene glycol) monomethyl ether as a colourless oil (79% yield). ^{1}H NMR (300 MHz, $CDCl_3$): δ 1.25–1.40 (m. 12 H), 1.57 (t, $J = 6.8$ Hz, 2 H), 2.04 (m, 2 H), 3.37 (s, 3 H), 3.44 (t, $J = 6.9$ Hz, 2 H), 3.50–3.70 (m. 24 H), 4.90–5.10 (m, 2 H), 5.75–5.90 (m, 1 H).

2.2.2. Succinimidyl-10-undecenoate

Succinimidyl-10-undecenoate was prepared as described previously [37].

2.2.3. 1-Aminohexa(ethylene glycol) and 1-aminohexa(ethylene glycol) monomethyl ether

1-Amino hexa(ethylene glycols) were prepared as described previously [23].

2.3. Porous silicon rugate filter formation

Rugate filters with 60 sinusoidally varying refractive index layers and a porosity variation from 64% to 66% were prepared as described previously [35]. Briefly, silicon wafers were contacted at the back with a stainless steel electrode and etched in an electrochemical cell containing 25% ethanolic HF and a platinum ring electrode. The current density profile during anodic etching was computer-controlled. After anodization, the porous silicon wafer was rinsed thoroughly with ethanol, pentane and dried under a stream of nitrogen.

2.4. Monolayer formation

The freshly prepared hydride-terminated porous silicon rugate filters were derivatized with Si–C linked monolayers by hydrosilylation of alkenes by immersing the rugate filters under positive pressure of argon in a 0.2 M solution of the alkene in mesitylene or 1,3,5-triethylbenzene for 16 h at 160 °C in a flame dried Schlenk flask. The alkene solution contained 20 mM triethylsilyl chloride as an in situ drying agent [38,39].

2.5. Coupling of aminated hexa(ethylene glycol) derivatives to NHS ester terminated monolayers.

Coupling of H_2N-EG_6R (R = Me, H) to terminal NHS esters was achieved by immersion of the *N*-succinimidyl undecenoate modified porous silicon rugate filters in a 20 mM solution of the amine in ethyl acetate for 4 h at room temperature.

2.6. Protein assay

Porous silicon samples were wetted with ethanol,[1] rinsed with water and incubated in a solution of fluorescein labelled bovine serum albumin (FITC-BSA), 1 mg/mL, in phosphate buffered saline (1 × PBS) (pH 7.4) for 1 h in the dark followed by copious rinsing with MilliQ water. The samples were then incubated overnight in elution buffer ((1 × SSPE) containing 1% 2-mercaptoethanol (v/v), 1% Triton X-100 (v/v), pH 7.4), heated at 40 °C for 2 h and the fluorescence of the elution buffer was measured. Standard curves were generated over 0–1 mg/mL and the solutions subjected to the same conditions of incubation for the samples ($R^2 > 0.999$).

2.7. Stability experiment

Porous silicon samples were incubated in phosphate buffered saline (1 × PBS) (pH 7.4) at 37 °C while reflectivity measurements (in buffer) were taken over time.

2.8. Spectroscopy

The optical reflectivity spectra were measured at normal incidence using a J/Y SPEX 1681 spectrometer, and a silicon detector. The infrared (FTIR) spectra were measured with a ThermoNicolet AVATAR 370-FTIR spectrometer. Fluorescence spectra were obtained using a Perkin Elmer LS 50 B Fluorometer.

[1] Water does not enter the pores of porous silicon modified with hydrophobic monolayers (such as the C12 monolayer). To ensure infiltration of aqueous solutions, the samples were first wetted with ethanol.

3. Results and discussion

3.1. Effect of surface chemistry on photonic resonance

Fig. 2 shows the optical reflectivity spectra of the freshly etched rugate filter (0) and after hydrosilylation of alkene (4) and subsequent coupling of H_2NEG_6 (4b), demonstrating a red-shift in the resonance after addition of organic layers. Table 1 lists the shifts in resonance position commonly observed for each chemical species. Hydrosilylation of the C12 (1) molecule resulted in a larger shift ($\Delta\lambda$, 29 nm) than that observed for OEG (2–3) molecules ($\Delta\lambda$, 20–24 nm) despite the OEG being a significantly larger molecule and hence filling more of the void space in the pores. Previous work on pure alkyl monolayers on silicon have demonstrated tight alkyl packing with surface coverage of ~0.5 molecules per surface silicon atom [18,39,40]. Studies of molecules containing OEG moieties have suggested a significantly lower packing density (<0.4 molecules per silicon atom) at the hydrophobic monolayer base. The different regions within the molecule are expected to pack differently upon hydrosilylation thus limiting the density of alkyl chains at the base of the monolayer by the configuration of OEG moieties in the pores [31,32]. A higher grafting density for pure alkyl monolayers would account for the larger shift in the reflectivity observed compared to a less dense OEG monolayer.

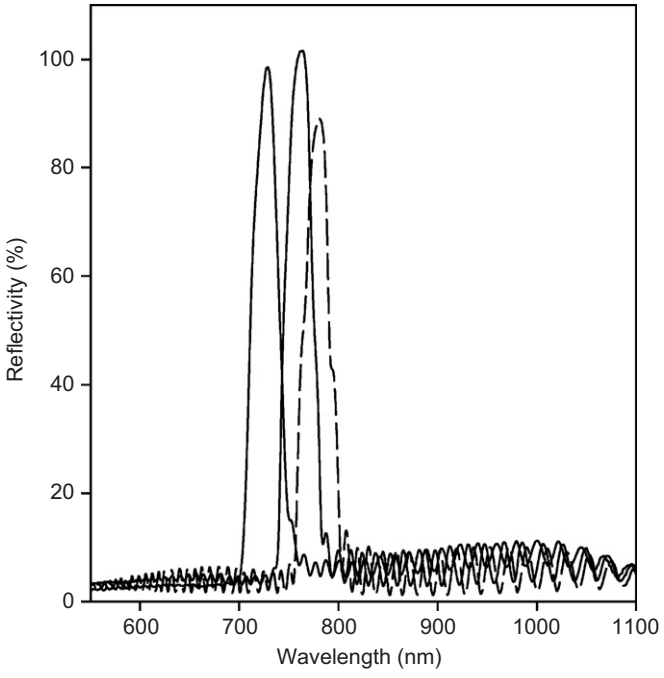

Fig. 2. Optical filter resonance and subsequent red-shifts in position upon hydrosilylation of NHS undecenoate (4). Dotted line displays the secondary shift after coupling of EG_6 amines (4b).

This lower surface density of the OEG molecules on the silicon surface (<0.4 molecules per surface silicon atom) implies there will be a higher degree of unprotected silicon. To determine the role that grafting density plays in stabilizing the porous silicon, the second strategy was developed (Fig. 1, Strategy 2). Firstly a dense alkyl monolayer is formed by hydrosilylation of NHS undecenoate [37] (molecule 4, resulting in a large reflectivity shift comparable to C12 (1) ($\Delta\lambda$, 29–34 nm)) to provide protection from oxidation. Subsequently, protein resistance is afforded by coupling an OEG containing amine to the active head group (Strategy 2, (4a)/(4b)). Secondary chemical modification of the active NHS terminated monolayer (4) with H_2NEG_6 produces an additional red-shift of 13–19 nm (Fig. 2 (4b) dotted line). Assuming the optical shifts in the resonance are proportional to the amount of immobilized molecules in the PSi, the secondary shifts correspond to 45–55% coupling of H_2NEG_6 to the NHS monolayer, which is in good agreement with previous reports utilizing this surface chemistry on Si(1 1 1) [37].

3.2. Infrared characterization of organic layers

To investigate the quality of the monolayers, spectral reflectance Fourier transform infrared (FTIR) spectroscopy was performed at each chemical modification step. Fig. 3 shows the IR absorbance for PSi samples modified with the different chemical entities. The top spectrum (0) displays the silicon hydride stretching of the freshly etched surface (Si–H_x, $x = 1, 2, 3$) at 2068–2200 cm^{-1} and Si-H_2 bending at 910 cm^{-1}. Hydrosilylation of C12 (1) results in the appearance of –CH_2 and –CH_3 stretching at 2928 cm^{-1}/2856 cm^{-1} (asymmetric/symmetric) and 2962 cm^{-1}, respectively with –CH_2 scissor mode at 1469 cm^{-1}, evidence of monolayer formation. Hydrosilylation of $C11EG_3Me$ (2) and $C11EG_6Me$ (3) results in the appearance of similar spectral peaks ($C11EG_3Me$ (2), –CH_2 asym./sym./sciss.: 2925/2856/1456 cm^{-1}. $C11EG_6Me$ (3), –CH_2 asym./sym./

Table 1
High reflectivity optical shift of rugate filters from freshly grown to modified with organic layers

Surface	Reflectivity shift (nm)
(1) C12	29
(2) C11–EG_3Me	20
(3) C11–EG_6Me	24
(4a) C10–C(O)O–NHS/–C(O)NH–EG_6Me	29/13[a]
(4b) C10–C(O)O–NHS/–C(O)NH–EG_6	34/19[a]

[a]Alkene hydrosilylation shift/coupling of OEG amine shift (multiple step procedure Scheme 2).

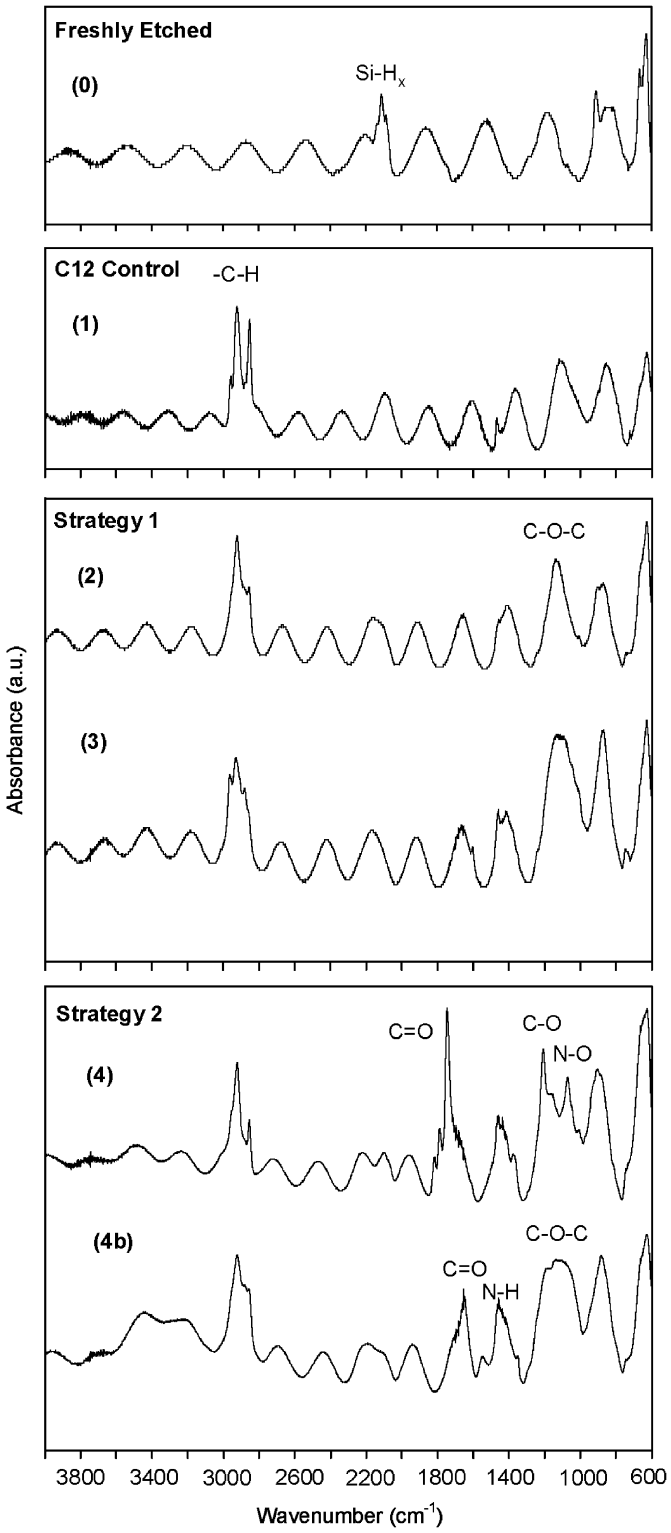

Fig. 3. Fourier transform infrared spectra of each surface formed after hydrosilylation of (1) C12, (2) $C11EG_3Me$, (3) $C11EG_6Me$ and (4) NHS undecanoate. Spectrum (4b) shows surface (4) after coupling of EG_6 amine.

sciss.: 2933/2882/1456 cm^{-1}) with the presence of –C–O/–C–C stretching of the ethylene oxide moieties at ~1130–1140 cm^{-1}. The position of EG spectral modes can be used to qualitatively assess the conformation of OEG chains [33]. Both molecules display non-crystalline mode positions such that protein resistance is favourable [33]. Some silicon dioxide on the surface is evident by the lower wavenumber shoulder to the OEG peak at ~1050–1100 cm^{-1} attributed to surface oxidation by adventitious water during hydrosilylation.

Fig. 3, Strategy 2 (4) shows the spectrum of the surface modified with the NHS ester terminated alkyl chains, indicated by the asymmetric and symmetric $–CH_2$ modes (2926 and 2857 cm^{-1}) with the additional appearance of an NHS carbonyl species at 1750 cm^{-1} and adjacent succinimide peaks (1792, 1823 cm^{-1}). The –C–O stretch at 1077 cm^{-1} and N–O stretch at 1214 cm^{-1} are also readily apparent. Reaction of H_2NEG_6 (4b) leads to disappearance of the NHS peaks with evidence of amide bond formation by the Amide I (carbonyl stretch) and II (N–H bend) peaks at 1652 and 1558 cm^{-1}. In addition, the asymmetric/symmetric $–CH_2$ stretching shifts/broadens (2927/2851–2899 cm^{-1}) upon coupling with the incorporation of the EG moiety and we see the appearance of terminal hydroxide –OH stretching at 3200–3300 cm^{-1}. The characteristic mode of the OEG ether stretch is ~1100 cm^{-1}. The relatively broad peak from the OEG (~1100 cm^{-1}) is attributed to contributions from SiO_2 (~1050 cm^{-1}) stretching due to some surface oxidation during the coupling of H_2NEG_6 (4b).

3.3. Stability under physiological conditions

To evaluate the stability of the different surface chemistries, PSi samples were incubated for extended periods of time in phosphate buffered saline at 37 °C. Freshly etched silicon samples oxidized rapidly with gas evolution, dissolving within 8 h. Fig. 4a shows the reflectivity position of the rugate filter resonance for single step surfaces $C11EG_3Me$ (2), $C11EG_6Me$ (3) and multiple step surface $C10C(O)NH–EG_6Me$ (4a). Both single step surfaces oxidized readily with loss of the photonic signal within 2 days. Fig. 4b shows the blue shift and drop in reflectivity for surface (3). The rapid decay in reflectivity is consistent with the proposed model of insufficient grafting density at the monolayer base, allowing water to penetrate the monolayer and oxidize/dissolve the silicon. Similar results were observed for surface (2). The PSi filters modified with the multiple step procedure showed a remarkable increase in stability (Fig. 4c). There was a steady blue shift attributed to oxidation over 5 days leading to the decrease in reflectivity (~−22.1 nm/day) observed in Fig. 4a (inset: 5 day linear trend, $R^2 = 0.997$) after which a resonance position plateau was reached. Thereafter, the sample oxidized much more slowly (~−0.2 nm/day) and the filter resonance was measurable for up to 2 months. Dissolution of the porous silicon was evident visually by colour change after 1 month. However, sufficient material remained to provide the photonic resonance upon interrogation until after 60 days, whereupon the porous film dissolved completely.

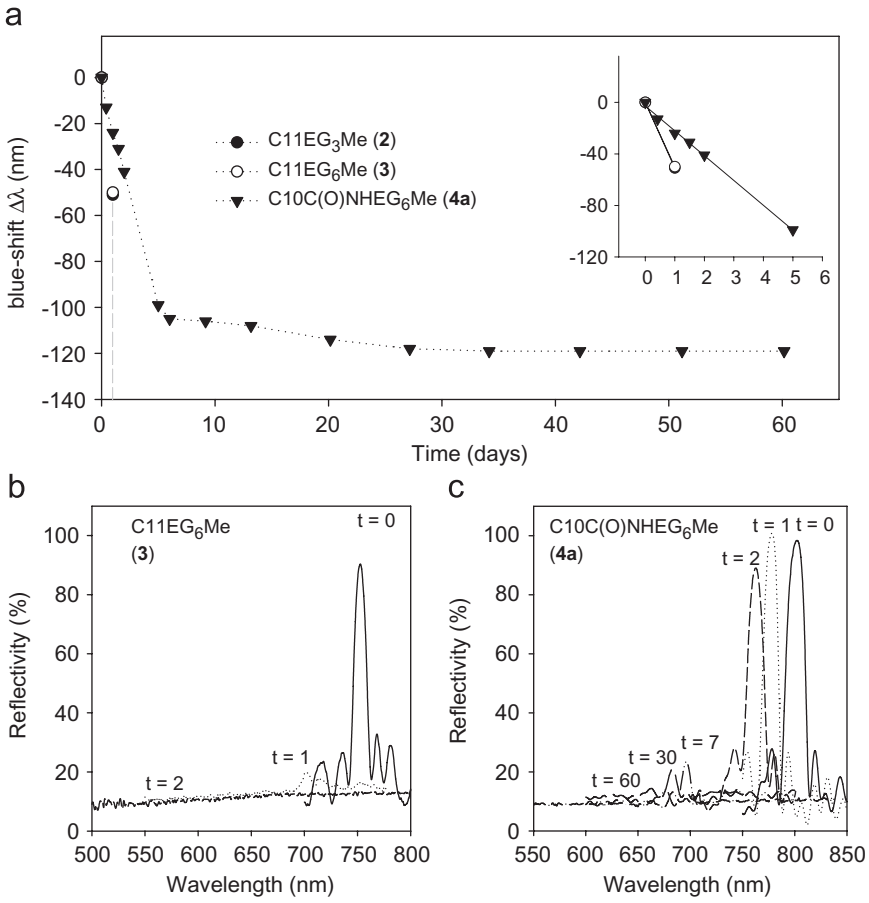

Fig. 4. High reflectivity resonance position shift of rugate filters under physiological conditions: (a) position over time for both Scheme 1 (surfaces (2) and (3)) and Scheme 2 (surface 4a). (b) depiction of drop in resonance amplitude with prolonged exposure for $C11EG_6Me$ (3) and (c) multiple step $C10C(O)NHEG_6Me$ (4a).

The improved stability with this scheme is attributed to the higher grafting density of alkyl chains at the surface protecting the underlying silicon from the ingress of water. The initial change in reflectivity over the first few days is believed to be due to oxidation of silicon hydride species $Si–H_x$ ($x = 1, 2, 3$) that did not react with alkene [41]. Dissolution of these regions lowers the refractive index of the PSi, leading to a blue-shift in the filter resonance. After initial oxidation of the porous film, a slower dissolution of silicon occurs over time, mediated by the intervening organic layer. Maintaining a reflectivity resonance under these conditions for a timescale of months is quite surprising. Chemical passivation throughout the structure effectively stabilizes the photonics by slowing oxidation and dissolution. Uniform chemical coverage promotes a homogeneous degradation of the structure thus allowing optical measurements to be gathered until complete collapse of the film.

Silicon and OEG materials are biodegradable, the by-products are non-toxic and for some biomaterial applications, dissolution of the silicon is often desirable. Measuring the optical signature of subcutaneous/intravenous implanted porous silicon devices is possible (owing to the optical window of tissue [36]) and natural degradation of the material will eliminate the need for downstream surgical removal. For example, porous silicon photonic crystals could be integrated into an implant surface to

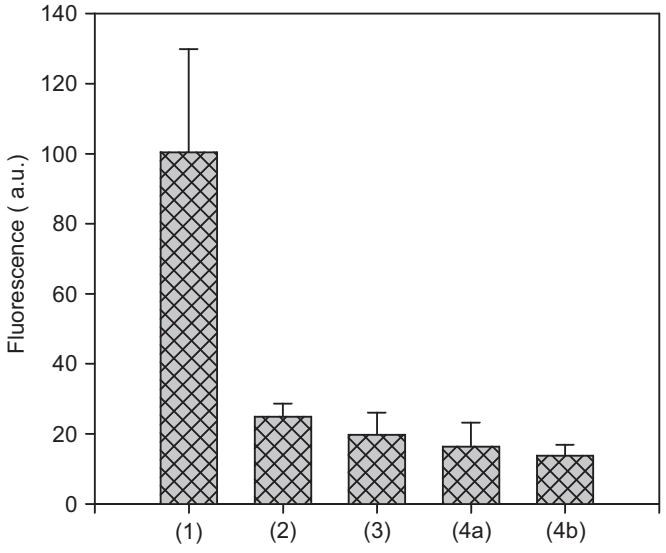

Fig. 5. Raw fluorescence of eluted FITC-BSA from surfaces (1)–(4a) and (4b).

Table 2
Protein adsorption and resistance of organic layers relative to C12 as 100% adsorbed (s = standard deviation, n = number of replicates)

Surface	Protein adsorbed (μg/cm^2)	Protein resistance (%)
(1) C12	0.065 ($s = 0.018$, $n = 3$)	—
(2) C11–EG_3Me	0.015 ($s = 0.002$, $n = 3$)	75
(3) C11–EG_6Me	0.012 ($s = 0.003$, $n = 4$)	80
(4a) C10–C(O)O–NHS/–C(O)NH–EG_6Me	0.010 ($s = 0.004$, $n = 4$)	84
(4b) C10–C(O)O–NHS/–C(O)NH–EG_6	0.008 ($s = 0.001$, $n = 3$)	86

monitor the local environment during wound healing. When monitoring the implant becomes unnecessary, the silicon dissolves and is cleared by the body. The exquisite control of surface chemistry could allow for many different moieties of practical interest to be incorporated into the surface layers and the chemistry adjusted such that biodegradability is controlled.

3.4. Reduction in non-specific protein adsorption

After assessing the passivation capabilities of these strategies, the ability to resist protein adsorption was examined by incubating the surface in a solution containing fluorescent protein (fluorescein labelled bovine serum albumin, FITC-BSA) followed by elution from the surface and quantification using a technique reported previously for flat silicon [23,30]. Fig. 5 shows the fluorescence of eluted material from the porous silicon filters. All surfaces modified with OEG containing molecules had less protein on the surface than the C12 surface (as determined by elution). Table 2 lists the mass of eluted protein per PSi internal surface area.[2] The C12 interface adsorbed 0.065 μg/cm^2 corresponding to 83% of a monolayer of BSA. A close-to-complete coverage was expected for hydrophobic surfaces. The hydrophilic OEG interfaces adsorbed 10–20% of a BSA monolayer. Table 2 lists the corresponding percent reduction in adsorbed protein relative to the C12 (1) layer as a model interface for maximum protein adsorbed. The 2-step strategy (4b) with terminal hydroxyl functionality performed the best with >87% reduction in adsorbed protein with little sample-to-sample variability. All four interfaces show resistance to protein adsorption with a trend from (4b) > (4a) > (3) > (2). Surface (4b) displayed improved resistance to (2) (2 population t-test, P-value 0.05) while other interfaces behaved comparably. EG_6 terminated surfaces resisted comparable amounts (81–87%) to our previous work on flat Si(1 0 0) (90% with undecenoic acid control [23]). There was little improvement afforded with terminal hydroxyl functionality ((4a) versus (4b)), suggesting terminal hydrophilicity does not play as large of a role as on flat substrates. The -EG_3Me surface adsorbed less than 20% of a monolayer, consistent with previous results on flat Si(1 1 1) [32].

[2]Internal surface area of PSi photonic crystals was determined by assuming cylindrical pores of average diameter 50 nm and 60-layer film thickness of 10 μm (by SEM). Maximum BSA coverage was approximated assuming close packing of the molecule (average diameter 9.3 nm, BSA dimensions $4 \times 10 \times 14$ nm^3).

4. Conclusions

Incorporating OEG moieties into alkene monomers for hydrosilylation was found to be amenable to porous silicon photonic crystals as an interface for passivating the underlying silicon and reducing non-specific protein adsorption. The two-step strategy provided a >30-fold enhancement of stability when exposed to physiological temperatures and pH, eventually dissolving after 60 days. Protein resistance was comparable to previous work providing >75% reduction in adsorbed bovine serum albumin with similar antifouling behaviour for the different strategies. Developing a robust chemistry to increase the physiological stability of photonic crystals and resist fouling caused by proteins will assist their development towards biosensors and components of ''smart'' biomaterials for external monitoring of implantable devices.

Acknowledgements

We would like to thank Dr. Jason Harper for assistance with synthetic methods and the Australian Research Council for Funding.

References

[1] Chen S, Zhu Z, Zhu J, Jian Z, Shi Y, Ke Y, et al. Hydroxyapatite coating on porous silicon substrate obtained by precipitation process. Appl Surf Sci 2004;230(1–4):418–24.
[2] Chin V, Collins BE, Sailor MJ, Bhatia SN. Compatibility of primary hepatocytes with oxidized nanoporous silicon. Adv Mater (Weinheim, Germany) 2001;13(24):1877–80.
[3] Low SP, Williams KA, Canham LT, Voelcker NH. Evaluation of mammalian cell adhesion on surface-modified porous silicon. Biomaterials 2006;27(26):4538–46.
[4] Sapelkin AV, Bayliss SC, Unal B, Charalambou A. Interaction of B50 rat hippocampal cells with stain-etched porous silicon. Biomaterials 2006;27(6):842–6.
[5] Janshoff A, Dancil K-PS, Steinem C, Greiner DP, Lin VSY, Gurtner C, et al. Macroporous p-type silicon Fabry–Perot layers. Fabrication, characterization, and applications in biosensing. J Am Chem Soc 1998;120(46):12108–16.
[6] Pacholski C, Sartor M, Sailor MJ, Cunin F, Miskelly GM. Biosensing using porous silicon double-layer interferometers:

reflective interferometric Fourier transform spectroscopy. J Am Chem Soc 2005;127(33):11636–45.
[7] Dancil K-PS, Greiner DP, Sailor MJ. A porous silicon optical biosensor: detection of reversible binding of IgG to a protein A-modified surface. J Am Chem Soc 1999;121(34):7925–30.
[8] Ouyang H, Christophersen M, Viard R, Miller BL, Fauchet PM. Macroporous silicon microcavities for macromolecule detection. Adv Funct Mater 2005;15(11):1851–9.
[9] Chan S, Horner SR, Fauchet PM, Miller BL. Identification of Gram negative bacteria using nanoscale silicon microcavities. J Am Chem Soc 2001;123(47):11797–8.
[10] DeLouise LA, Kou PM, Miller BL. Cross-correlation of optical microcavity biosensor response with immobilized enzyme activity. Insights into biosensor sensitivity. Anal Chem 2005;77(10):3222–30.
[11] Ryu C-S, Cho SM, Kim B-W. Interferometric sensing of b-galactosidase released by recombinant *E. coli* responding to an endocrine disruptor, tributyltin. Biotechnol Lett 2001;23(9): 653–9.
[12] Di Francia G, La Ferrara V, Lancellotti L, Quercia L. Porous silicon based gas sensors. Recent Res Dev Electrochem 2000;3(Part 1): 93–106.
[13] Galeazzo E, Peres HEM, Santos G, Peixoto N, Ramirez-Fernandez FJ. Gas sensitive porous silicon devices: responses to organic vapors. Sensors Actuators, B: Chem 2003;B93(1–3):384–90.
[14] Marsh G. Porous silicon a useful imperfection. Mater Today (Oxford, United Kingdom) 2002;5(1):36–41.
[15] Raissi F, Farivar R. Room-temperature hydrogen gas sensor. Appl Phys Lett 2005;87(16):164101/1–3.
[16] Saha H, Pramanik C. Porous silicon-based sensors: prospects and challenges. Mater Manuf Process 2006;21(3):239–46.
[17] Buriak JM. Organometallic chemistry on silicon and germanium surfaces. Chem Rev (Washington, DC) 2002;102(5):1271–308.
[18] Boukherroub R, Wojtyk JTC, Wayner DDM, Lockwood DJ. Thermal hydrosilylation of undecylenic acid with porous silicon. J Electrochem Soc 2002;149(2):H59–63.
[19] Letant SE, Hart BR, Kane SR, Hadi MZ, Shields SJ, Reynolds JG. Enzyme immobilization on porous silicon surfaces. Adv Mater (Weinheim, Germany) 2004;16(8):689–93.
[20] Canham LT, Reeves CL, Newey JP, Houlton MR, Cox TI, Buriak JM, et al. Derivatized mesoporous silicon with dramatically improved stability in simulated human blood plasma. Adv Mater (Weinheim, Germany) 1999;11(18):1505–7.
[21] Canham LT, Stewart MP, Buriak JM, Reeves CL, Anderson M, Squire EK, et al. Derivatized porous silicon mirrors: implantable optical components with slow resorbability. Phys Status Solidi A: Appl Res 2000;182(1):521–5.
[22] Böcking T, Kilian KA, Gaus K, Gooding JJ. Single-step DNA immobilization on antifouling self-assembled monolayers covalently bound to silicon (111). Langmuir 2006;22(8):3494–7.
[23] Kilian KA, Böcking T, Ilyas S, Gaus K, Gal M, Gooding JJ. Forming antifouling organic multilayers on porous silicon rugate filters towards in vivo/ex vivo biophotonic devices. Adv Funct Mater 2007, in press.
[24] Prime KL, Whitesides GM. Adsorption of proteins onto surfaces containing end-attached oligo(ethylene oxide): a model system using self-assembled monolayers. J Am Chem Soc 1993;115(23):10714–21.
[25] Yam C-M, Xiao Z, Gu J, Boutet S, Cai C. Modification of silicon AFM cantilever tips with and oligo(ethylene glycol) derivative for resisting proteins and maintaining a small tip size for high-resolution imaging. J Am Chem Soc 2003;125(25):7498–9.
[26] Yam CM, Lopez-Romero JM, Gu J, Cai C. Protein-resistant monolayers prepared by hydrosilylation of a-oligo(ethylene glycol)-w-alkenes on hydrogen-terminated silicon(1 1 1) surfaces. Chem Commun (Cambridge, United Kingdom) 2004(21):2510–1.
[27] Gu J, Yam CM, Li S, Cai C. Nanometric protein arrays on protein-resistant monolayers on silicon surfaces. J Am Chem Soc 2004; 126(26):8098–9.
[28] Lasseter TL, Clare BH, Abbott NL, Hamers RJ. Covalently modified silicon and diamond surfaces: resistance to nonspecific protein adsorption and optimization for biosensing. J Am Chem Soc 2004;126(33):10220–1.
[29] Yam CM, Gu J, Li S, Cai C. Comparison of resistance to protein adsorption and stability of thin films derived from a-hepta-(ethylene glycol) methyl w-undecenyl ether on HSi(1 1 1) and HSi(1 0 0) surfaces. J Colloid Interf Sci 2005;285(2):711–8.
[30] Clare TL, Clare BH, Nichols BM, Abbott NL, Hamers RJ. Functional monolayers for improved resistance to protein adsorption: oligo(ethylene glycol)-modified silicon and diamond surfaces. Langmuir 2005;21(14):6344–55.
[31] Böcking T, Kilian KA, Hanley T, Ilyas S, Gaus K, Gal M, et al. Formation of tetra(ethylene oxide) terminated Si–C linked monolayers and their derivatization with glycine: an example of a generic strategy for the immobilization of biomolecules on silicon. Langmuir 2005;21(23):10522–9.
[32] Böcking T, Gal M, Gaus K, Gooding JJ. Evidence for why tri(ethylene oxide) functionalized Si–C linked monolayers on Si(1 1 1) have inferior protein antifouling properties relative to the equivalent alkanethiol monolayers assembled on gold. Aust J Chem 2005;58(9):660–3.
[33] Harder P, Grunze M, Dahint R, Whitesides GM, Laibinis PE. Molecular conformation in oligo(ethylene glycol)-terminated self-assembled monolayers on gold and silver surfaces determines their ability to resist protein adsorption. J Phys Chem B 1998;102(2): 426–36.
[34] Herrwerth S, Eck W, Reinhardt S, Grunze M. Factors that determine the protein resistance of oligoether self-assembled monolayers—internal hydrophilicity, terminal hydrophilicity, and lateral packing density. J Am Chem Soc 2003;125(31):9359–66.
[35] Ilyas S, Böcking T, Kilian K, Reece PJ, Gooding J, Gaus K, et al. Porous silicon based narrow line-width rugate filters. Opt Mater 2007;29(6):619–22.
[36] Matcher SJ, Cope M, Delpy DT. In vivo measurements of the wavelength dependence of tissue-scattering coefficients between 760 and 900 nm measured with time-resolved spectroscopy. Appl Opt 1997;36(1):386–96.
[37] Böcking T, James M, Coster HGL, Chilcott TC, Barrow KD. Structural characterization of organic multilayers on silicon(1 1 1) formed by immobilization of molecular films on functionalized Si–C linked monolayers. Langmuir 2004;20(21):9227–35.
[38] Boukherroub R, Morin S, Sharpe P, Wayner DDM, Allongue P. Insights into the formation mechanisms of Si-OR monolayers from the thermal reactions of alcohols and aldehydes with Si(1 1 1)–H. Langmuir 2000;16(19):7429–34.
[39] Boukherroub R, Morin S, Wayner DDM, Bensebaa F, Sproule GI, Baribeau JM, et al. Ideal passivation of luminescent porous silicon by thermal, noncatalytic reaction with alkenes and aldehydes. Chem Mater 2001;13(6):2002–11.
[40] Cicero RL, Linford MR, Chidsey CED. Photoreactivity of unsaturated compounds with hydrogen-terminated silicon(1 1 1). Langmuir 2000;16(13):5688–95.
[41] Allongue P, Costa-Kieling V, Gerischer H. Etching of silicon in sodium hydroxide solutions. II. Electrochemical studies of *n*-silicon(1 1 1) and (1 0 0) and mechanism of the dissolution. J Electrochem Soc 1993;140(4):1018–26.